

基于高 Q 值轴向渐变型空芯微腔的高灵敏流速传感器

万洪丹*, 张帅, 陈或芳, 张疏桐, 汪静丽, 施伟华

南京邮电大学电子与光学工程学院、柔性电子(未来技术)学院, 江苏 南京 210023

摘要 创新性地提出了一种基于高 Q 值轴向渐变型空芯微腔的高灵敏流速传感器, 实现了微压状态下微腔回音壁模式共振光场对流体的直接检测。首先, 利用流体动力学和有限元算法理论分析了轴向渐变型空芯微腔的流速和光场特性。其次, 通过熔融拉锥和气压控制法制备了高 Q 值($Q > 10^7$)轴向渐变型空芯微腔, 利用五维高精度位移平台实现微腔与微纳光纤的高精度、低损耗耦合。实验测试并研究了不同尺寸、不同耦合位置时微腔回音壁模式共振光谱的流速传感特性, 获得的最大流速灵敏度达 $0.27 \text{ pm}/(\mu\text{L}/\text{min})$, 流速分辨率为 $1.43 \mu\text{L}/\text{min}$ 。该传感器具有较高的重复性和实时性, 在高灵敏度流体检测、水质检测等领域具有潜在应用价值。

关键词 轴向渐变型空芯微腔; 流速传感; 回音壁模式; 灵敏度; 分辨率

中图分类号 O43; TG502.33; TN256

文献标志码 A

DOI: 10.3788/AOS230977

1 引言

从生化检测到国防安全保护的各个领域, 流速检测都发挥着重要作用^[1-3], 特别是微流控技术已广泛应用于细胞和生物分子检测、药物筛选、化学合成和分析等研究中^[4-6], 比如, 在流式细胞术中, 流速控制着计数以及生物药物的细胞黏附和单克隆抗体产生^[7-10]。目前已开发了多种流速传感器, 如电磁流速计^[11]、涡街流速计^[12]和超声波流速计^[13]等。其中: 电磁流速计只能测量导电液体的流速^[10]; 涡街流速计无法测量较低的流速信号, 且信号检测过程相对复杂^[14]; 超声波流速计的性能受到温度和压力变化的影响^[15]。光纤流速传感器因具备尺寸紧凑、抗电磁干扰强、高灵敏度等特点, 有效解决了流速检测局限性、信号检测复杂和易受温度、压力影响等问题^[2, 16-17]。Morshed 等^[2]提出了一种单模-多模-单模光纤结构的光纤流速传感器, 该传感器具有光信号可检测性和传感器操作简单的优势。Allil 等^[16]提出一种基于光纤布拉格光栅、互相关技术的流速传感器, 该系统采用廉价的组件开发, 侵入性小, 并且不受压力和温度的影响。Lv 等^[17]提出了一种可同时测量流速和温度的光纤传感器, 具有体积小、灵敏度高、测量范围宽、压力损失小等优势。

光纤流速传感器大多是将光纤作为悬臂梁放置在

流体中, 当受到流动流体的作用时, 光纤中影响光传输的相关物理参数(强度、波长、频率或相位)发生改变, 从而实现流速感知与测量^[18-19]。光纤流速传感器根据传感模式主要可分为透射式和反射式, 当前使用较多的传感元件则为光纤布拉格光栅(FBG)和掺杂光纤, 其实际应用中需要结合特殊设计的微流控通道和封装结构^[20-22], 且流速测量分辨率有限^[16, 23]。因此, 目前仍然需要实现灵敏度高、分辨率高、结构简单、成本低的流速传感检测。

回音壁模式(WGM)光学微腔^[24]具有 Q 值高、模式体积小和光场密度高等特点, 在非线性光学^[25]、激光器^[26]和高灵敏度光学传感器^[27-28]等领域中备受关注^[29-30]。与微流体技术结合使用时, 空芯光学微腔由于本身可作微流控通道、高 Q 值和强光-物质相互作用等优势, 在高精度流体检测等生化传感方面具有广泛的应用^[31]。Chen 等^[32]提出一种基于伯努利效应的微泡腔流速传感器, 流速灵敏度可达 $0.0196 \text{ pm}/(\mu\text{L}/\text{min})$, 并从理论上分析了伯努利效应引起的流体压力变化。为了提升灵敏度, Wang 等^[33]提出一种高灵敏度光学微腔流速传感器, 该传感器基于流体伯努利效应以及激发高阶径向模式将流速灵敏度提高到 $0.079 \text{ pm}/(\mu\text{L}/\text{min})$ 。然而, 流速灵敏度仍有提升空间, 且高阶径向模式对耦合条件要求高、激发效率相对较低^[34-35]。

收稿日期: 2023-05-15; 修回日期: 2023-06-10; 录用日期: 2023-06-15; 网络首发日期: 2023-06-25

基金项目: 国家自然科学基金(12174199, 11704199)、中国博士后科学基金(2021M701765)、江苏省自然科学基金面上项目(BK20221330)、江苏省青蓝工程优秀青年骨干教师计划、南京邮电大学 STITP 项目、江苏省研究生实践创新计划项目(SJ CX21_0275)

通信作者: *hdwan@njupt.edu.cn

本文提出一种基于轴向渐变型空芯微腔(GHM)的流速传感器,首次实现了微压条件下微腔 WGM 共振光场对流体流速的直接检测。首先,基于计算流体动力学(CFD)算法和有限元算法分析了 GHM 的流体流速和光场理论物理模型。其次,通过调控工艺参数的熔融拉锥和气压控制法制备了高 Q 值 GHM,结合高精度多维耦合方法实现其与微纳光纤的高精度、低损耗耦合,激发随流速实时变化的 WGM 共振光谱,实验测试了不同耦合位置以及微腔尺寸决定的流速传感特性。最后,采用轴向渐变型结构增大微腔 WGM 光场与流场的相互作用,获得了高达 $0.27 \text{ pm}/(\mu\text{L}/\text{min})$ 的流速灵敏度,分辨率为 $1.43 \mu\text{L}/\text{min}$ 。该传感器具有较好的重复性和实时性,在高灵敏度流体检测、水质检测等领域具有较高的应用价值。

2 理论与实验

2.1 传感机制理论分析

通过 Ansys 中 Fluent 模块的 CFD 算法,对具有不同径长比(横向直径 L 和轴向长度 Z 之比)的 GHM 和突变型空芯微腔(MHM)进行腔内流速理论仿真分析

与对比。图 1(a)和(b)为 GHM 和 MHM 的 3D 结构模型,其中,两种微腔耦合区域外径 $L_1=L_3=190 \mu\text{m}$,内径 $L_2=L_4=186 \mu\text{m}$,且 GHM 的渐变区轴向长度 $Z_1=4800 \mu\text{m}$,MHM 的突变区轴向长度 $Z_2=210 \mu\text{m}$ 。

图 1(c)和(d)分别为通入溶液流速为 $75 \mu\text{L}/\text{min}$ 时,两种结构的轴截面(左上图)和横截面(右下图)流速仿真结果。可以看出:轴截面上,MHM 流速的变化高于 GHM,且经过 MHM 突变区流速远远高于 GHM;横截面上,MHM 的管壁区域流速较低,管中心的流速较高,而对于 GHM,整体管中流速差别较小。图 1(e)为 GHM 和 MHM 中流体实际流速数值图比较,可以看出:距离(与微腔横截面中心点 O 的距离)为 $-45\sim 45 \mu\text{m}$ (图中黄色区域)时,MHM 中的液体流速比 GHM 高;距离区间为 $-94\sim -45 \mu\text{m}$ 以及 $45\sim 94 \mu\text{m}$ (图中灰色区域)时,GHM 中的液体流速比 MHM 高。特别地,在图 1(e)的子图中,对于 GHM 来说,靠近管壁外侧(即远离微腔横截面中心点 O ,此位置受到的压力很小)仍然有可测的流速信息。因此,相比于突变结构,本文提出的渐变结构微腔用于实现流速传感时具有更好的有效性。

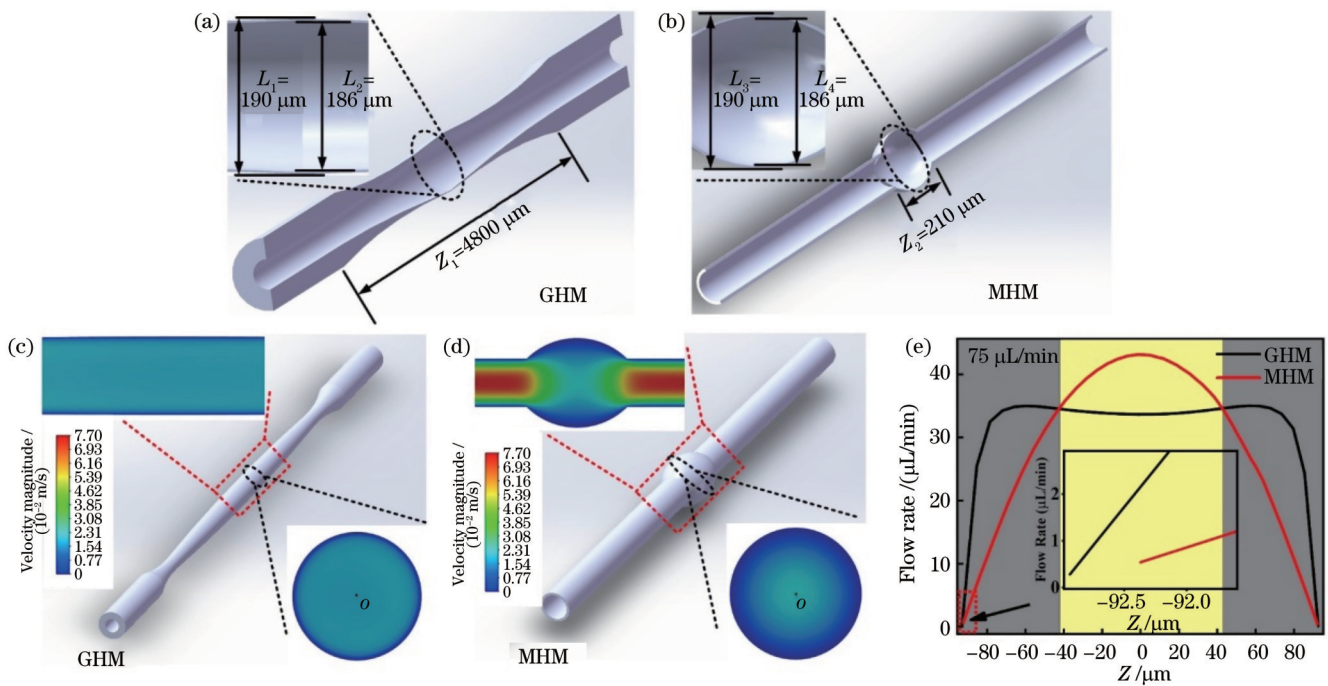


图 1 GHM 和 MHM 的流速仿真比较。(a)(b)结构模型;(c)(d)流场分布图(左上角和右下角为图中模型虚线处的流场细节);(e)横截面流速比较

Fig. 1 Comparison of flow rate simulation of GHM and MHM. (a)(b) Structural model; (c)(d) flow field distribution (upper left and lower right images are the flow field details at the dashed line of the model); (e) comparison of cross section flow rate

2.2 GHM 的结构详细分析

为了更好地描述 GHM 在流速传感过程中实际的情况,通过 CFD 算法对 GHM 的不同位置进行了仿真,如图 2(a)所示。图中对 GHM 的 4 个部位进行了分析(1 为入口处,2 为凹陷处,3 为传感区横截面,4 为

传感区轴截面)。首先,从入口处来看,结构为一般的管道结构,因此流速并没有特别明显的变化;其次,在凹陷处,由于此处管道内径相比入水口较小,因此液体通过此处时会有一定的聚集,造成了通过此处液体流速的增强;由于 GHM 的特殊结构(弧度小且弧度区域

管道长),传感区的横截面和轴截面的流速变化并不明显,这有利于在液体通过过程中,实现对流速减少的减缓,保持了传感区的流速。而MHM的流速更多保持在腔内,且腔壁流速很小[图1(d)]。这更多是由于管的结构引起:由于管鼓起间隔较短且鼓起部分弧度较大,流速强的位置更多集中在管中,管壁位置流速更小,虽然更利于对于管壁的压力检测(伯努利原理:管壁流速减小,其静压增大)^[32],但并不能实现流速的直接检测。除此之外,通过Comsol有限元

算法仿真了不同微腔管壁厚度决定的WGM光场特性(由于计算机运行内存和网格精度的限制,微腔尺寸小于实验中实际微腔的尺寸,即外径 L 设置为 $15\ \mu\text{m}$,壁厚 d 为 $1\sim 5\ \mu\text{m}$,网格精度为 $20\ \text{nm}$)。从图2(b)可以看出,随着管壁厚度的减小,光场会不断向腔内移动,表明腔壁厚度的减小有利于增强光场与腔内物质的作用强度。而在整体GHM结构[图2(a)]中,传感区域的管壁最薄,因此在该处可对流速进行有效检测。

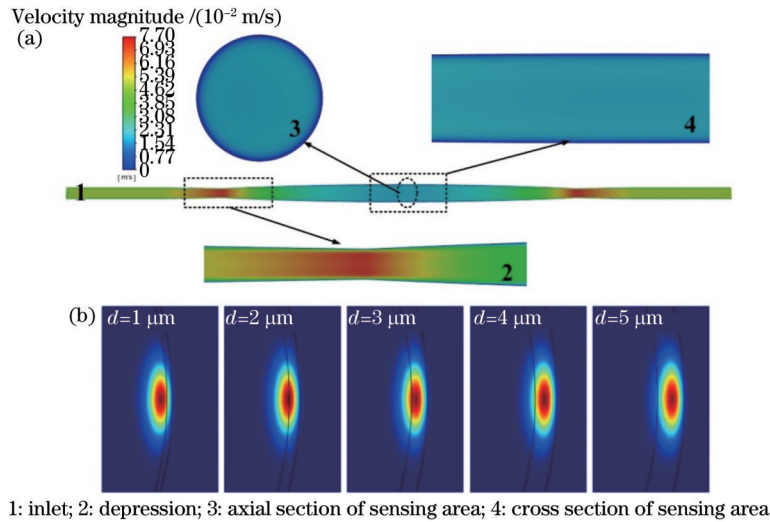


图2 GHM 流速仿真。(a) $75\ \mu\text{L}/\text{min}$ 流速下流场分布图;(b) 不同壁厚的GHM光场分析

Fig. 2 Flow rate simulation of the GHM. (a) Specific flow field distribution diagram with flow rate of $75\ \mu\text{L}/\text{min}$; (b) optical field analysis of the GHM with different wall thicknesses

为了探究流速对于管道压力的影响,通过计算流体动力学算法分析了流速在 $15\ \mu\text{L}/\text{min}$ 下GHM的压力分布。图3(a)为整体管道表面的动态压力分布,图3(b)为传感区域横截面处的压力分布,可以看出整体

结构的流速对于管壁的压力很小,均在 $1\times 10^{-3}\ \text{Pa}$ 左右。总体来看,流体对腔壁的压力很小,因此该流速传感过程为微压状态。

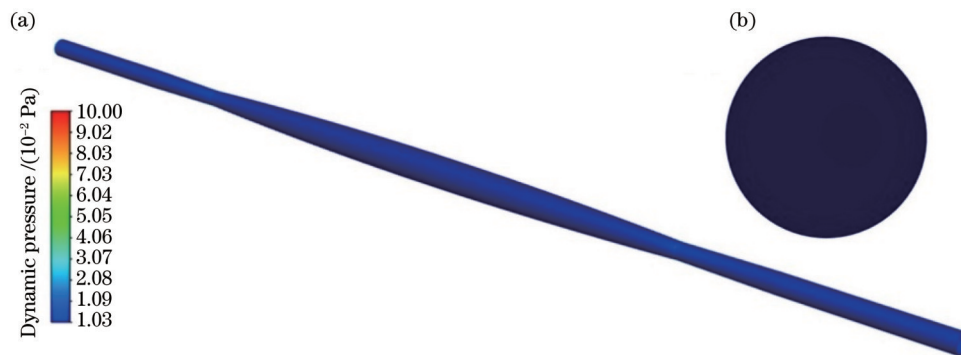


图3 $15\ \mu\text{L}/\text{min}$ 流速下GHM的压力分布。(a)整体表面;(b)传感区域横截面

Fig. 3 GHM pressure distribution with flow rate of $15\ \mu\text{L}/\text{min}$. (a) Overall surface; (b) cross section of sensing area

3 GHM的制备与其表征

如图4(a)所示,该GHM的制备分为3个过程:1)将毛细管去除中间部分,并将尾端通过紫外胶封装;2)通过操控拉锥机,选择适合参数进行熔融拉锥;3)当

运行到一定的时间时,关闭程序,此时微腔表面呈现微微鼓起的状态。图4(b)为GHM的显微镜实物图片,图中标注为该腔的最大外径处尺寸 $L=190\ \mu\text{m}$ 。图4(c)为基于GHM的流速传感实验系统装置图。衰减器将可调谐窄带激光器(TLS,CTL 1550,中心波长为

1550 nm, 线宽 < 5 kHz, 调谐范围为 35 GHz) 发出的光衰减后再和微腔进行耦合, 偏振控制器调控光路的整体偏振态。GHM 和锥形光纤通过光学紫外胶进行耦合封装, 通过控制蠕动泵来控制进出 GHM 的溶液速度。光电探测器将经过的光转换为电信号送入到反

馈系统中进行处理得到回音壁模式共振光谱。图 4(d) 为实验测得 GHM 回音壁模式共振光谱, 图 4(e) 为图 4(d) 中红色方框中的放大细节图的洛伦兹拟合, 根据 $Q = \lambda / \Delta\lambda$ 计算可得, 中心波长为 1549.99374 nm 处的 Q 值为 1.79×10^7 。

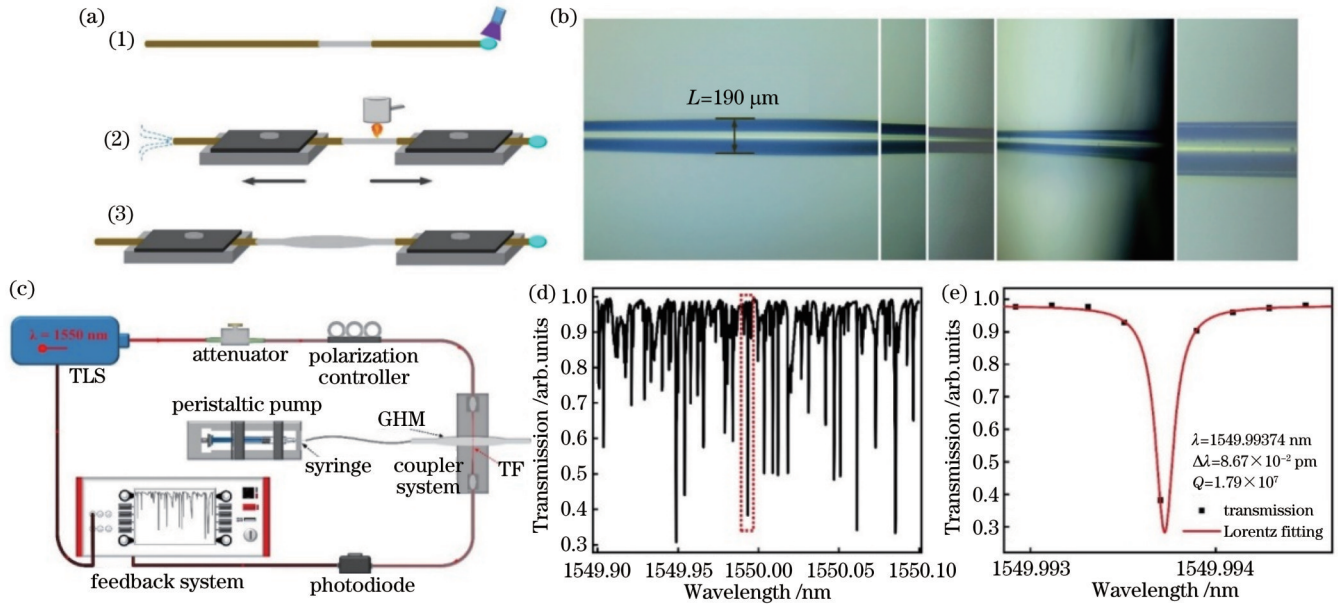


图 4 GHM 的制备及其表征。(a) 制备过程; (b) 实物图; (c) 实验装置示意图; (d) WGM 光谱; (e) Q 值

Fig. 4 Preparation and characterization of the GHM. (a) Fabrication process; (b) physical map; (c) schematic diagram of experimental setup; (d) WGM spectrum; (e) Q value

4 基于 GHM 的高灵敏度流速传感实验

4.1 同一耦合位置不同共振波长流速传感

实验过程中通入液体为超纯水溶液, 通过调整蠕动泵 (TJ-3A, 最小流速为 $7 \mu\text{L}/\text{min}$) 参数控制通入液体流速 (流速为 $15 \mu\text{L}/\text{min}$ 、 $30 \mu\text{L}/\text{min}$ 、 $45 \mu\text{L}/\text{min}$ 、 $60 \mu\text{L}/\text{min}$ 、 $75 \mu\text{L}/\text{min}$)。更换流速过程中需断开蠕动泵待流速降为 0。首先, 对 GHM 同一耦合位置不同共振波长处的流速传感特性进行了研究。根据微腔灵敏度 S ^[36] 公式为

$$S = \frac{\Delta\lambda}{\Delta n} \approx \frac{\lambda}{n_2} \eta_3, \quad (1)$$

式中: λ 为 WGM 的中心波长; n_2 为微腔的折射率; η_3 表示 WGM 在管内液芯的能量占比。由式 (1) 可知, 传感器的灵敏度主要与 WGM 中心波长、微腔折射率和 WGM 在液芯区域能量分布的大小有关。由于相同微腔同一耦合位置处的微腔折射率和能量占比相同, 随着共振波长的增加, 其流速灵敏度会得到一定的增强。

图 5(a) 为同一耦合位置 (耦合直径 $L = 190.61 \mu\text{m}$) 不同流速下的 WGM 光谱实验测试结果, 6 种不同颜色的箭头代表不同共振波长处的回音壁模式光谱, 分别为 1549.94877、1549.97820、1549.99669、

1550.03174、1550.04269、1550.05214 nm。从图 5(a) 可以看出, 共振波长随着流速的增加而向长波长偏移。图 5(b) 显示了 GHM 的不同回音壁模式共振波长与流速的线性拟合关系。结果表明, 6 个不同波长的共振传感特性都具有良好的线性度 ($R^2 > 0.9$), 且灵敏度分别为 0.169、0.178、0.198、0.205、0.230 $\text{pm}/(\mu\text{L}/\text{min})$ 。图 5(c) 为 WGM 光谱的不同共振波长与灵敏度的关系, 可以看出, 随着波长的增加, 流速传感灵敏度增加。

4.2 同一 GHM 不同耦合位置流速传感

其次, 对同一个 GHM 不同耦合位置的传感特性进行了研究。选取了 GHM 的 5 个不同位置, 其外径分别为 120.46、156.20、174.75、182.69、190.61 μm 。图 6(a) 显示了 GHM 的不同耦合位置的 WGM 波长漂移与流速的线性拟合关系, 可以看出, 不同外径处 (120.46、156.20、174.75、182.69、190.61 μm) 的流速灵敏度分别为 0.037、0.095、0.134、0.177、0.230 $\text{pm}/(\mu\text{L}/\text{min})$ 。图 6(b) 为不同外径的流速灵敏度对比结果。随着微腔外径的增大, 流速灵敏度的变化呈现非线性增大, 流速灵敏度最大值 ($L = 190.61 \mu\text{m}$) 与最小值 ($L = 126.46 \mu\text{m}$) 相差约 6 倍, 其拟合公式为 $y = 0.021 + 0.023 \times \exp[(x - 126.287)/29.521]$ 。出现这种现象的原因是随着 GHM 外径的增加, 腔内壁的厚度会减小, WGM 在管

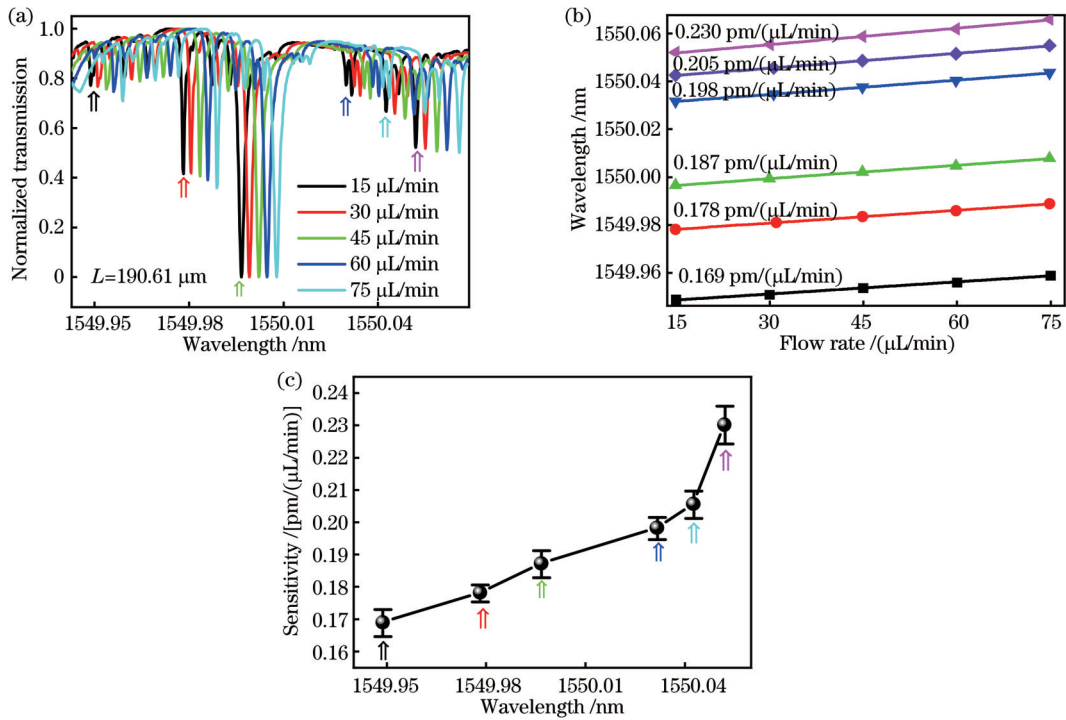


图5 同一耦合位置不同共振波长流速测量结果。(a) 不同流速下的WGM光谱;(b) WGM共振波长与流速的关系;(c) 不同共振波长处的流速灵敏度

Fig. 5 Flow rate measurement results at different resonance wavelengths of the same coupling position. (a) WGM spectra at different flow rates; (b) relationship between WGM resonance wavelength and flow rate; (c) flow rate sensitivity at different resonance wavelengths

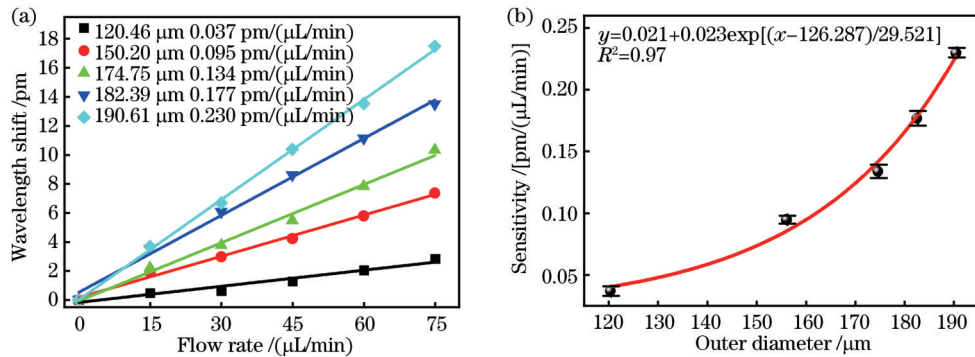


图6 同一GHM不同位置流速测试结果。(a) 共振波长漂移与流速的关系;(b) 流速灵敏度

Fig. 6 Flow rate measurement results at different positions of the same GHM. (a) Relationship between resonance wavelength shift and flow rate; (b) flow rate sensitivity

内液芯的能量占比变大,即增大了式(1)中的 η_3 ,由此实现了流速灵敏度的增强。

4.3 不同最大外径的GHM流速传感

为了探究不同尺寸GHM的传感特性,实验研究了3种不同最大外径(174.73、190.61、221.06 μm)的GHM流速传感特性。图7(a)不同最大外径的GHM的共振波长与流速的线性拟合关系,其中最大外径为174.73、190.61、221.06 μm 时流速灵敏度分别为0.180、0.230、0.270 $\text{pm}/(\mu\text{L}/\text{min})$ 。如图7(b)所示,流速灵敏度随着GHM最大外径的增大而增大。由于外径的增大导致管壁厚度的减小,WGM在管内液芯的能量占比增加,光场与液体之间的相互作用增强。

4.4 传感器的稳定性和分辨率

首先测试了该传感器的稳定性。将溶液通入微腔中静置,等待腔内流速降低为0后检测WGM共振光谱的变化。图8为管内流速为0时WGM共振光谱的漂移情况,测试时间为1h以上。结果表明,在1h内波长的漂移量 $< \pm 0.12500$ pm,标准偏差 σ 为0.12873 pm。根据分辨率公式 $R = 3\sigma/S$ (其中,S为测得的流速灵敏度)计算可得,该微腔的流速分辨率为1.43 $\mu\text{L}/\text{min}$ 。

4.5 传感器的实时性和重复性

图9(a)为该流速传感器的实时性检测结果,在检测不同流速过程中不断开蠕动泵进行连续性检测,实

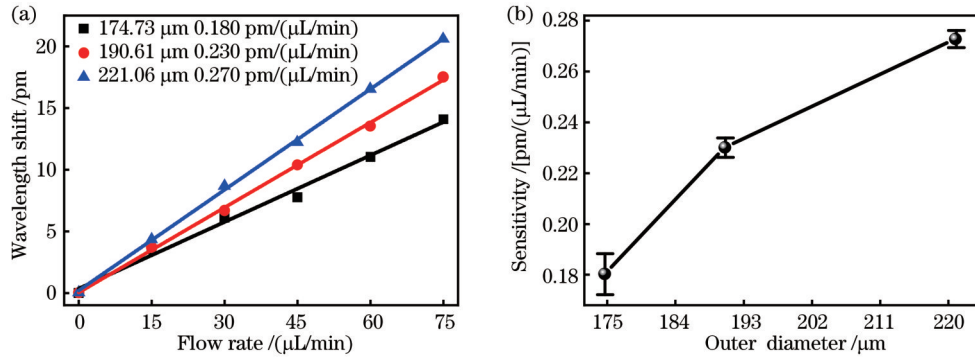


图 7 不同外径的 GHM 流速测试结果。(a) 共振波长漂移与流速的关系;(b) 流速灵敏度

Fig. 7 Flow rate measurement results of GHM with different outer diameters. (a) Relationship between resonance wavelength shift and flow rate; (b) flow rate sensitivity

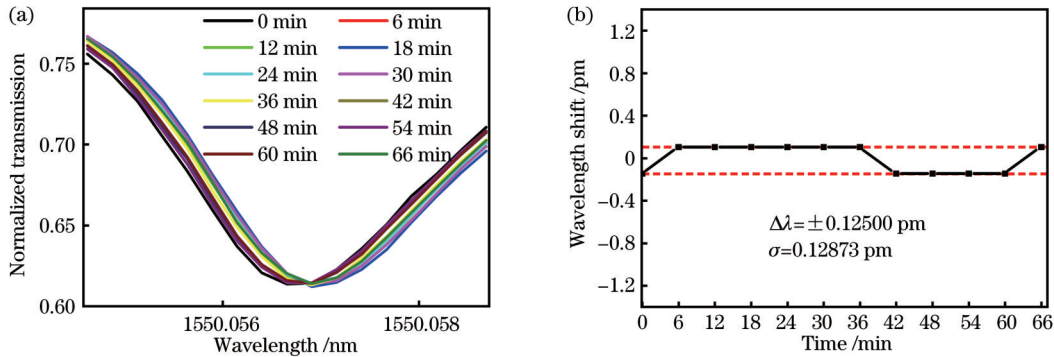


图 8 GHM 稳定性测试结果。(a) 回音壁谱的变化;(b) 波长漂移与时间的关系

Fig. 8 Stability test results of GHM. (a) Variation of WGM spectra; (b) relationship between wavelength shift and time

际检测过程中发现开始时波长会微小红移(约为 0.40 pm),且持续时间短(约为 30 s)。该红移是在注射器连接过程中在 GHM 腔内形成小的内压导致液体的流动所产生,这也说明了该传感器具有较高的流速检测灵敏度。此外,随着流速的增大,关闭蠕动泵至稳定阶段的波长会有一定的红移(15 $\mu\text{L}/\text{min}$ 关系泵稳定后的波长红移量为 0.9 pm,75 $\mu\text{L}/\text{min}$ 后的波长红移量为 1.20 pm),其原因可能是微腔本身的热效应、水

流对管内的冲击压力效应等。

通过 24 h 内相同微腔在稳定流速(75 $\mu\text{L}/\text{min}$)下的 WGM 光谱变化检测了传感器的重复性,检测过程中不断地开关蠕动泵,观测 WGM 共振光谱的漂移,结果如图 9(b)所示。图中标注出开关蠕动泵的时间节点。实验结果表明,在打开和关闭蠕动泵的操作过程中,该传感器的波长漂移对腔内流速的变化具有较好的快速响应能力。

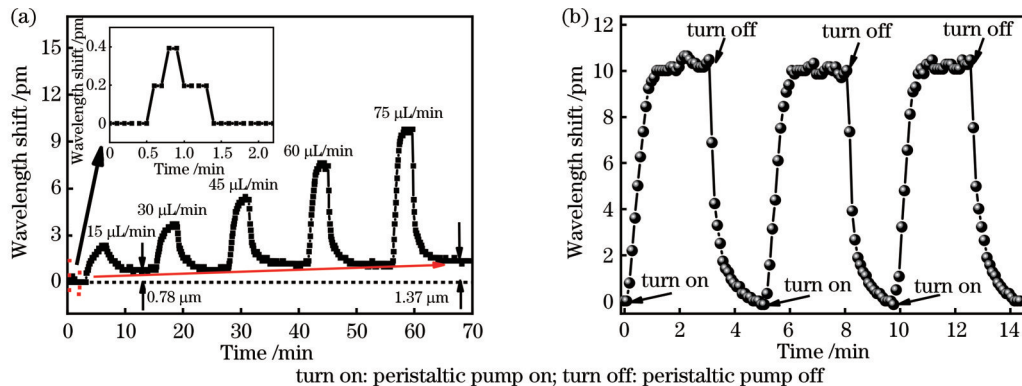


图 9 传感器的实时性和重复性测试结果。(a) 不同流速下 GHM 的波长漂移;(b) 75 $\mu\text{L}/\text{min}$ 流速下重复性测试结果

Fig. 9 Real-time and repeatability test results of the sensor. (a) Wavelength shift of GHM at different velocities; (b) repeatability test result at flow rate of 75 $\mu\text{L}/\text{min}$

表 1 列出了不同光学类流速传感器的灵敏度和分辨率对比,可以看出,本文提出的 GHM 流速传感器的

灵敏度和分辨率在微腔类和悬臂梁式流速传感中都具有较好的性能。

表 1 不同光学类流速传感器性能对比

Type	Flow rate / ($\mu\text{L}/\text{min}$)	Sensitivity / [$\text{pm}/(\mu\text{L}/\text{min})$]	Shift direction	Resolution / ($\mu\text{L}/\text{min}$)	Ref.
Microbubble	0-200	1.96×10^{-2}	Blue shift	—	[32]
Microvial	0-200	7.90×10^{-2}	Blue shift	—	[33]
PDMS micro cantilever beam type	0-600	—	Cantilever beam deformation increases	35	[38]
FBG cantilever beam type	0-6000	1.53×10^5	Red shift	324	[39]
GHM	0-75	0.27	Red shift	1.43	Proposed

5 结 论

本文提出了一种基于轴向渐变型空芯微腔的高灵敏流速传感器,首次实现了微压状态下微腔回音壁模式共振光场对流体的直接检测。基于流体动力学算法和有限元算法对 GHM 的流速、光场进行了理论分析,利用熔融拉锥和气压控制法制备了 GHM。通过多维高精度耦合激发高 Q 值 WGM 共振光谱,通过实时监测 WGM 光谱变化实现了高灵敏度流速测试。采用轴向渐变型结构增大微腔 WGM 光场与流场相互作用,获得了最大流速灵敏度为 $0.27 \text{ pm}/(\mu\text{L}/\text{min})$ 、分辨率为 $1.43 \mu\text{L}/\text{min}$ 的高性能流速传感器。该流速传感器具有较好的重复性和实时性,在流体传感、水质检测、医用检测等领域具有潜在应用价值。

参 考 文 献

- [1] Kam S I. Mechanistic modeling of pipeline leak detection at fixed inlet rate[J]. *Journal of Petroleum Science and Engineering*, 2010, 70(3/4): 145-156.
- [2] Morshed A H, Atta R, Packirisamy M. Fluidic flow measurement using single mode - multimode - single mode optical fiber sensor[J]. *IEEE Sensors Journal*, 2021, 21(12): 13316-13326.
- [3] Kumar J S, Kamaraj A, Sundaram C K, et al. A comprehensive review on accuracy in ultrasonic flow measurement using reconfigurable systems and deep learning approaches[J]. *AIP Advances*, 2020, 10(10): 105221.
- [4] de Carvalho C B, de Carvalho E P, da Silva Sá Ravagnani M A. Optimization of flow rate distribution in a crude oil preheat train considering fouling deposition in shell and tube sides[J]. *Industrial & Engineering Chemistry Research*, 2022, 61(16): 5568-5577.
- [5] Wu F, Wang H P, Wang C Y, et al. A hydraulic model for flow rate ratio of triple cannulation extracorporeal membrane oxygenation[J]. *Physics of Fluids*, 2022, 34(4): 041703.
- [6] Gong Y, Liu Q F, Zhang C L, et al. Microfluidic flow rate detection with a large dynamic range by optical manipulation[J]. *IEEE Photonics Technology Letters*, 2015, 27(23): 2508-2511.
- [7] Hassan U, Watkins N N, Edwards C, et al. Flow metering characterization within an electrical cell counting microfluidic device[J]. *Lab on a Chip*, 2014, 14(8): 1469-1476.
- [8] Garza-García L D, García-López E, Camacho-León S, et al. Continuous flow micro-bioreactors for the production of biopharmaceuticals: the effect of geometry, surface texture, and flow rate[J]. *Lab on a Chip*, 2014, 14(7): 1320-1329.

- [9] Stan C A, Tang S K Y, Whitesides G M. Independent control of drop size and velocity in microfluidic flow-focusing generators using variable temperature and flow rate[J]. *Analytical Chemistry*, 2009, 81(6): 2399-2402.
- [10] Gupta H, Arumuru V, Jha R. Industrial fluid flow measurement using optical fiber sensors: a review[J]. *IEEE Sensors Journal*, 2021, 21(6): 7130-7144.
- [11] Mitchell B, Zhou Y W, Hayes M P, et al. Non-invasive groundwater velocity measurements using a novel electromagnetic flowmeter[J]. *IEEE Transactions on Instrumentation and Measurement*, 2022, 71: 2000515.
- [12] Thummar D, Reddy Y J, Arumuru V. Machine learning for vortex flowmeter design[J]. *IEEE Transactions on Instrumentation and Measurement*, 2022, 71: 1001708.
- [13] Johnson A N, Harman E, Boyd J T. Blow-down calibration of a large ultrasonic flow meter[J]. *Flow Measurement and Instrumentation*, 2021, 77: 101848.
- [14] Venugopal A, Agrawal A, Prabhu S V. Note: a vortex cross-correlation flowmeter with enhanced turndown ratio[J]. *Review of Scientific Instruments*, 2014, 85(6): 066109.
- [15] Lynnworth L C, Liu Y. Ultrasonic flowmeters: half-century progress report, 1955-2005[J]. *Ultrasonics*, 2006, 44: e1371-e1378.
- [16] Allil A S, da Silva Dutra F, Dante A, et al. FBG-based sensor applied to flow rate measurements[J]. *IEEE Transactions on Instrumentation and Measurement*, 2021, 70: 7000608.
- [17] Lv R Q, Zheng H K, Zhao Y, et al. An optical fiber sensor for simultaneous measurement of flow rate and temperature in the pipeline[J]. *Optical Fiber Technology*, 2018, 45: 313-318.
- [18] Martincek I, Kacik D, Horak J. Interferometric optical fiber sensor for monitoring of dynamic railway traffic[J]. *Optics & Laser Technology*, 2021, 140: 107069.
- [19] Wang J, Liu Z Y, Gao S R, et al. Fiber-optic anemometer based on Bragg grating inscribed in metal-filled microstructured optical fiber[J]. *Journal of Lightwave Technology*, 2016, 34(21): 4884-4889.
- [20] Liu Z G, Wang F, Zhang Y, et al. Low-power-consumption fiber-optic anemometer based on long-period grating with SWCNT coating[J]. *IEEE Sensors Journal*, 2019, 19(7): 2592-2597.
- [21] Baroncini V H V, Martelli C, da Silva M J, et al. Single- and two-phase flow characterization using optical fiber Bragg gratings [J]. *Sensors*, 2015, 15(3): 6549-6559.
- [22] Pang Y N, Liu B, Liu J, et al. Singlemode-multimode-singlemode optical fiber sensor for accurate blood pressure monitoring[J]. *Journal of Lightwave Technology*, 2022, 40(13): 4443-4450.
- [23] Liu G G, Sheng Q W, Hou W L, et al. Optical fiber vector flow sensor based on a silicon Fabry - Perot interferometer array [J]. *Optics Letters*, 2016, 41(20): 4629-4632.
- [24] Foreman M R, Swaim J D, Vollmer F. Whispering gallery

- mode sensors[J]. *Advances in Optics and Photonics*, 2015, 7(2): 168-240.
- [25] 张新亮, 赵延著. 微腔光频梳研究进展[J]. *光学学报*, 2021, 41(8): 0823014.
Zhang X L, Zhao Y J. Research progress of microresonator-based optical frequency combs[J]. *Acta Optica Sinica*, 2021, 41(8): 0823014.
- [26] 樊碳润, 肖金龙, 杨跃德, 等. 回音壁微腔激光器电老化试验及寿命分析[J]. *中国激光*, 2022, 49(6): 0601001.
Fan Y R, Xiao J L, Yang Y D, et al. Electrical aging test and lifetime analysis of whispering-gallery-mode micro-cavity lasers [J]. *Chinese Journal of Lasers*, 2022, 49(6): 0601001.
- [27] 叶思放, 方云团. 基于 Parity-Time 对称耦合微腔的血糖传感器[J]. *中国激光*, 2022, 49(3): 0310002.
Ye S F, Fang Y T. Blood glucose sensor based on parity-time symmetry coupled cavities[J]. *Chinese Journal of Lasers*, 2022, 49(3): 0310002.
- [28] Zhang S, Wan H D, Xiong J X, et al. A high-Q, hollow-core micro-bottle cavity biosensor for DNA detection with low detection limit[J]. *Journal of Lightwave Technology*, 2022, 40(15): 5345-5351.
- [29] 余霞, 陈旭, 刘静敏, 等. 基于回音壁模式微腔的激光自注入锁定技术[J]. *中国激光*, 2022, 49(19): 1901001.
Yu X, Chen X, Liu J M, et al. Laser self-injection locking technology based on whispering gallery mode microcavity[J]. *Chinese Journal of Lasers*, 2022, 49(19): 1901001.
- [30] 王亚平, 王秀翊, 王璞. 回音壁模式光学微腔识别细胞类型[J]. *中国激光*, 2020, 47(2): 0207028.
Wang Y P, Wang X H, Wang P. Identifying single cell types via whispering gallery mode optical microcavities[J]. *Chinese Journal of Lasers*, 2020, 47(2): 0207028.
- [31] Zhao X Y, Guo Z H, Zhou Y, et al. Optical whispering-gallery-mode microbubble sensors[J]. *Micromachines*, 2022, 13(4): 592.
- [32] Chen Z M, Guo Z H, Mu X, et al. Packaged microbubble resonator optofluidic flow rate sensor based on Bernoulli Effect [J]. *Optics Express*, 2019, 27(25): 36932-36940.
- [33] Wang Z J, Zhang X B, Zhao S C, et al. High-sensitivity flow rate sensor enabled by higher order modes of packaged microbottle resonator[J]. *IEEE Photonics Technology Letters*, 2021, 33(12): 599-602.
- [34] Liu X L, Lu Q J, Fu L A, et al. Coupled-mode induced transparency via Ohmic heating in a single polydimethylsiloxane-coated microbubble resonator[J]. *Optics Express*, 2020, 28(7): 10705-10713.
- [35] Yang Y, Ward J, Chormaic S N. Quasi-droplet microbubbles for high resolution sensing applications[J]. *Optics Express*, 2014, 22(6): 6881-6898.
- [36] Zhu H Y, White I M, Suter J D, et al. Analysis of biomolecule detection with optofluidic ring resonator sensors[J]. *Optics Express*, 2007, 15(15): 9139-9146.
- [37] Chiavaioli F, Gouveia C, Jorge P, et al. Towards a uniform metrological assessment of grating-based optical fiber sensors: from refractometers to biosensors[J]. *Biosensors*, 2017, 7(4): 23.
- [38] Nezhad A S, Ghanbari M, Agudelo C G, et al. PDMS microcantilever-based flow sensor integration for lab-on-a-chip [J]. *IEEE Sensors Journal*, 2013, 13(2): 601-609.
- [39] Lu P, Chen Q Y. Fiber Bragg grating sensor for simultaneous measurement of flow rate and direction[J]. *Measurement Science and Technology*, 2008, 19(12): 125302.

Highly Sensitive Flow Rate Sensor Based on High Quality Graded Hollow-Core Microcavity

Wan Hongdan*, Zhang Shuai, Chen Yufang, Zhang Shutong, Wang Jingli, Shi Weihua
College of Electronic and Optical Engineering & College of Flexible Electronics (Future Technology), Nanjing University of Posts and Telecommunications, Nanjing 210023, Jiangsu, China

Abstract

Objective Flow rate detection plays an important role in various fields from biochemical detection to national defense security protection. In particular, microfluidics technology has been widely used in cell and biomolecular detection, drug screening, and chemical synthesis and analysis. Currently, various flow rate sensors have been developed, such as electromagnetic flow rate meters, vortex flow rate meters, ultrasonic flow rate meters, and fiber optic flow rate meters. Most of these flow rate meters have problems such as complex detection, susceptibility to interference, and limited flow resolution. Whispering gallery mode (WGM) optical microcavity has the characteristics of high Q value, small mode volume, and high optical field density, and it has attracted much attention in the field of high-sensitivity optical sensing. When combined with microfluidic technology, hollow optical microcavity can be used as a microfluidics channel, high Q value, and strong light matter interaction, so it has extensive research value in high-precision fluid detection and other biochemical sensors. However, there is still room for improvement in flow rate sensitivity. Moreover, higher-order radial modes require high coupling conditions and relatively low excitation efficiency. We propose a flow rate sensor based on graded hollow-core microcavity (GHM) with axial gradient, which achieves direct detection of fluids under micro-pressure conditions using the resonant light field of the microcavity. The sensor has excellent flow rate sensing performance and high application value in high-sensitivity fluid detection, water quality detection, and other fields.

Methods The distribution of fluid rate, pressure, and light field in GHM is analyzed theoretically by using the computational fluid dynamics (CFD) algorithm and finite element analysis of algorithms. High Q value GHM is fabricated.

GHM and tapered fiber are coupled precisely and packaged, WGM resonance spectrum is excited and varied according to the change of the flow rate in real time. The flow rate of the liquid is controlled by adjusting the parameters of the peristaltic pump (TJ-3A, the minimum flow rate is 7 $\mu\text{L}/\text{min}$) (flow rates are 15 $\mu\text{L}/\text{min}$, 30 $\mu\text{L}/\text{min}$, 45 $\mu\text{L}/\text{min}$, 60 $\mu\text{L}/\text{min}$, and 75 $\mu\text{L}/\text{min}$, respectively).

Results and Discussions Experimental results show that the resonance wavelength shifts towards a longer wavelength as the flow rate is increased (Fig. 5). This is because the sensitivity of the sensor is mainly related to the wavelength of the WGM spectra, the refractive index of the microcavity, and the energy distribution of the WGM in the liquid core region. As the resonance wavelength increases, the flow rate sensitivity will be enhanced. In addition, flow rate sensing is performed on GHMs with different coupling positions and outer diameters (Figs. 6 and 7). The results show that the flow rate sensitivity increases for the larger outer diameter of the GHM. By using an axial gradient structure to increase the interaction between the microcavity WGM light field and the flow field, high-performance flow rate sensing with a flow rate sensitivity of 0.270 $\text{pm}/(\mu\text{L}/\text{min})$ (Fig. 7) and a resolution of 1.43 $\mu\text{L}/\text{min}$ is obtained (Fig. 8). In addition, the sensor has great stability (Fig. 8) and fast response ability (Fig. 9).

Conclusions We propose and demonstrate a highly sensitive flow rate sensor based on high-quality graded hollow-core microcavity (GHM), which achieves direct detection of flow rate by the resonant light field of the microcavity's WGM oscillation with minimum intracavity pressure. Firstly, the flow rate and light field of the GHM are theoretically analyzed by fluid dynamics and finite element method. Secondly, GHM with a high Q value ($Q > 10^7$) is prepared by fused biconical tapering and gas pressure control methods. High Q WGM spectra are excited by high-precision and low-loss coupling between the microcavity and tapered fibers, with five dimensional high-precision displacement stages involved. The flow rate sensing characteristics of the proposed sensor are experimentally investigated by WGM spectra and measured with different cavity sizes and coupling conditions. The maximum flow rate sensitivity is measured to be 0.27 $\text{pm}/(\mu\text{L}/\text{min})$, with a flow rate resolution of 1.43 $\mu\text{L}/\text{min}$. This flow rate fiber sensor has high repeatability and real-time performance, and it has potential applications in various fields such as high-sensitivity fluid detection and water quality detection.

Key words graded hollow-core microcavity; flow rate detection; whispering-gallery mode; sensitivity; resolution